Journal of Petroleum Exploration and Production Technology (2023) 13:135–149
https://doi.org/10.1007/s13202-022-01541-x

ORIGINAL PAPER-EXPLORATION GEOPHYSICS

4D seismic co-processing pre-stack depth migration for scarce acquisition repeatability

Mohamed Mahgoub[1,2] · Yasir Bashir[1] · Andy Anderson Bery[1] · Abdel Wahab Noufal[2]

Received: 7 March 2022 / Accepted: 18 June 2022 / Published online: 19 July 2022

Abstract

Time-lapse (4D) seismic processing is routinely used to monitor hydrocarbon reservoir production. Seismic reflections are sensitive to formation pressure and fluid content. This means that repeated seismic surveys can theoretically detect pressure changes and fluid changes associated with field production. These measurements can help optimize production strategy and identify areas where hydrocarbons have been bypassed. However, the seismic signal associated with such changes can be negligible, especially in heterogeneous carbonate reservoirs. To measure this 4D signal, the seismic acquisition must be repeated. Data vintages should be processed together to minimize differences unrelated to production. Repeatability of data acquisition is sometimes impossible to achieve in the Middle East due to environmental changes (e.g., dunes, currents, field facilities). Due to high cost and inadequate sampling, attempts to permanently bury seismic sources and receivers have failed. In this study, least-square pre-stack depth migration (LSM) co-processing was applied to remove the influence of survey design on the final image and pinching mark compared to conventional Kirchhoff pre-stack depth migration (KPSDM). The 4D physical, geometric, and seismic attributes are analyzed in the field as key diagnostic tools to evaluate the probability of a sighted 4D difference independent of two different acquisition geometries. The 4D analysis was performed on two case studies offshore Abu Dhabi, to determine which workflow and algorithm are most likely to ensure that the complete and optimal 4D processing sequence relaxes the need for seismic acquisition repeatability.

Keywords 4D · Carbonate reservoir · Heterogeneous · Co-processing · Imaging

List of symbols

Acronym

LSM	Least-square migration
KPSDM	Kirchhoff pre-stack depth migration
PreSTM	Pre-stack time migration
PreSDM	Pre-stack depth migration
4D	Fourth dimension which is the time-lapse
RTM	Reverse time migration
LSTRM	Least-square reverse time migration
OBC	Ocean Bottom Cable
OBN	Ocean Bottom Node
TWT	Two-way time
COV	Common offset vector
PZ	P (hydrophone receiver which is pressure gradient) and while the collocated geophone is recording Z, the vector displacement of the seabed.
5D	Five dimensions; inline/crossline/offset/azimuth, and time dimension
RMS/NRMS	Root mean square/normalized root mean square
DSDR	Distance Source, Distance Receiver
OVTs	Offset vector tiles
Hz /DB	HZ is Hertz; frequency measuring unit. DB is Decibel; amplitude measuring unit

Nomenclature

d	The acquired seismic data
L	The acoustic operator of Kirchhoff modeling
r	The reflectivity of the subsurface
m	The Kirchhoff migrated image
L^H	The adjoint of the forward operator
r_{LS}	The subsurface reflectivity
L^HL	Hessian operator

✉ Yasir Bashir
dryasir.bashir@live.com

[1] School of Physics, Universiti Sains Malaysia, 11800 Penang, Malaysia

[2] Abu Dhabi National Oil Company (ADNOC), Abu Dhabi, UAE

f(r)	The least-squares cost function
Q	Compensation quality factor of seismic waves absorption
L_Q	Visco-acoustic Kirchhoff modeling operator
$(L^H L)^{-1}$	Inverse Hessian operator
RMS	Root mean square
NRMS	Normalized root mean square
a_i	Base survey trace
b_i	Monitor survey trace
t1 − t2	A given time window
C_{bm}	Cross-correlation of baseline and monitor trace within a time window
C_{bb}	Cross-correlation of baseline trace with itself
C_{mm}	Cross-correlation of monitor trace with itself
τ	Tau which is a constant value of 300
π	Pi is the ratio of the circumference of any circle to the diameter of that circle. In decimal form, the value of pi is approximately 3.14

Introduction

A time-lapse seismic survey is a repetition of 3D seismic surveys over a given area at different times. By comparing seismic data acquired over a field at two or more points in time, supplemented by well log data and production histories, time-lapse seismic allows observation of fluid pathways and pore fluid movement within reservoirs. The main advantage of 4D seismic is that it provides a comprehensive picture of fluid movement in the reservoir that well-specific monitoring techniques cannot capture. The 4D seismic datasets are a monitoring tool that allows you to track the dynamic changes in reservoirs during oil and gas production and/or injection activities. All surface effects unrelated to subsurface geology must be eliminated prior to 4D signal analysis. Interpretation of 4D seismic data focuses mainly on the differences in seismic images between the baseline and monitor surveys. The elastic properties of the reservoir may vary due to lithologic differences in the reservoir rocks, and 4D seismic co-processing is intended to minimize such lithologic differences. Seismic images, seismic inverted data, and wellbore information are used together to reliably explore reservoir properties. The 4D seismic co-processing tested in this study began with seismic data prior to 5D regularization for Case Study I, while it began with field tapes for Case study II. After 4D binning and matching the monitor to the baseline survey above the reservoir, the main focus was on the pre-stack depth migration workflow, where Kirchhoff pre-stack depth migration was tested against least-square Kirchhoff migration. 4D seismic metric attributes such as predictability, RMS, NRMS, and cross-correlation were analyzed as verifiers and diagnostic types of 4D analysis of seismic processing results. Standard pre-stack depth migration algorithms suffer from migration artifacts with void fluctuations, limited bandwidth, and distorted amplitude on subsurface reflectors (Gray 1997). This is true even for state-of-the-art imaging technology such as RTM (Zhang and Zhang 2009). Band-limited depth migration of primary reflectors often results in inadequate image illumination and resolution, due to limitations in both the acquisition geometry and the processing technology used (Liu et al. 2018). The applications of linear inversion in seismic imaging are well known (Schuster 1993; Nemeth et al. 1999; Prucha and Biondi 2002; Valenciano 2008). Standard pre-stack depth migration (PSDM), e.g., Kirchhoff/RTM, is unable to recover reflectivity with the expected amplitude fidelity and resolution fully. This is due to factors such as inhomogeneous subsurface illumination and irregular acquisition geometry (Shao et al. 2017). Time-lapse seismic images may be degraded if the reservoir overburden is complex or if the acquisition geometry deviates significantly between the baseline and the monitor acquisition (Ayeni and Biondi 2010). However, because LSM can remove acquisition effects, it is suitable for 4D imaging (Wang et al. 2017).

Least-squares migration (LSM) aims to recover the true reflectivity of the Earth by determining the inverse of the forward modeling operator through minimizing the square of the misfit between the recorded data and the modeled data (Huang et al. 2017). In addition, compared to traditional RTM and Fourier finite-difference migration, least-square reverse time migration (LSTRM) has good potential for use in reservoir description and four-dimensional (4D) seismic imaging (Xiao-Dong et al. 2017). Processing seismic time-lapse data is challenging when the acquired dataset contains inherent fluctuations that obscure the desired time-lapse signal (Fischer et al. 2013). The non-repeatable noise must be suppressed before the 4D signal becomes visible. Sources of non-repeatable noise often include variable amplitude gains, frequency content, static shifts, waveform phase changes, and positioning of events between different data vintages (Lumley et al. 2005). A common approach to addressing non-repeatable noise sources is to apply various adjustment filters to the datasets (Ross et al. 1996). The acquisition and processing of seismic data should ensure the repeatability of a seismic event concerning non-reservoir intervals. The only differential signal could be a phase change of the fluid in the reservoir. Therefore, data equalization and data conditioning at the non-reservoir level is extremely critical and important (Mitra et al. 2007). The main objective of this study is to evaluate the detectability of a 4D signal between two non-repeatable seismic surveys due to variations in acquisition and processing.

Study area and survey design

The major oil and gas fields in the Arabian Gulf, ranging in age from Permian to Tertiary, consist mainly of carbonates with evaporite seals formed in arid or semiarid climates with different stratigraphy, depositional conditions, and facies. This framework of erosion and flooding surfaces was formed by changes in sea level caused by epeirogenetic tectonic movements and eustatic history (Kendall and Alsharhan 2013). During the deposition of the reservoir formation, the area of the research oil field was located on a carbonate platform between the Arabian Shield and the Meso-Tethys Ocean, near the Qatar-Surmeh Arc, just south of the equator. The reservoir's carbonate–evaporite cycles result from progressive basin recharge that culminated in the establishment of supratidal sabkha conditions. The reservoir is part of a mega-sequence triggered in the late Callovian by significant flooding of the Middle East platform. This flooding was responsible for the deposition of the productive source rocks. During the Late Jurassic, sea level rose steadily while carbonate deposition kept pace with the flooding, creating increasingly shallow depositional conditions. The climate became arid and as shallowing progressed, evaporitic sabkha environments formed toward the end of the mega-sequence. The deposit is mainly limestone with some thin dolomite streaks, and the field is characterized by a bituminous zone that cuts through the deposit layers. Deterioration of porosity is observed in the bitumen zone and below it. Two case studies from offshore Abu Dhabi were used in this research. The first study (Case I) includes two surveys conducted 10 years apart with completely different designs. The pre-processing sequences were also very different, so that joint processing of the two surveys was only partial and did not begin until 4D binning. The second study (Case II) involved two surveys taken 20 years apart, again with completely different acquisition designs. In this case, however, full 4D co-processing took place between the two surveys. The study area is located offshore of Abu Dhabi in the United Arab Emirates in Case I. In 2010, the baseline seismic survey was conducted as a stand-alone 3D Ocean Bottom Cable (OBC) seismic survey with orthogonal geometry of overlapping zippers (Fig. 1a). On the other hand, the 2020 monitoring survey was conducted as part of a large seismic offshore 3D OBN (Ocean Bottom Node) block with a parallel geometry layout. The field covers a shallow water area where the water depth is approximately 6 and 22 m (Fig. 1b).

The two case studies have distinctly different acquisition configurations. Table 1 summarizes all the acquisition parameters, which clearly show that the geometry's spread layout, line intervals, receiver station spacing, and fold of the baseline survey are different, compared to the monitor measurements with different offsets.

This Case I field has been producing oil from Jurassic reservoirs since 1987 and has low relief with a four-way dip at a depth of approximately 9400 feet (2850 m) and a two-way time (TWT) of 1.5 s, and the reservoir has a strong bright spot (Fig. 2). There are multiple wells for production or water injection penetrating the crest of the reservoir, and different strings for many of these wells for different reservoir levels.

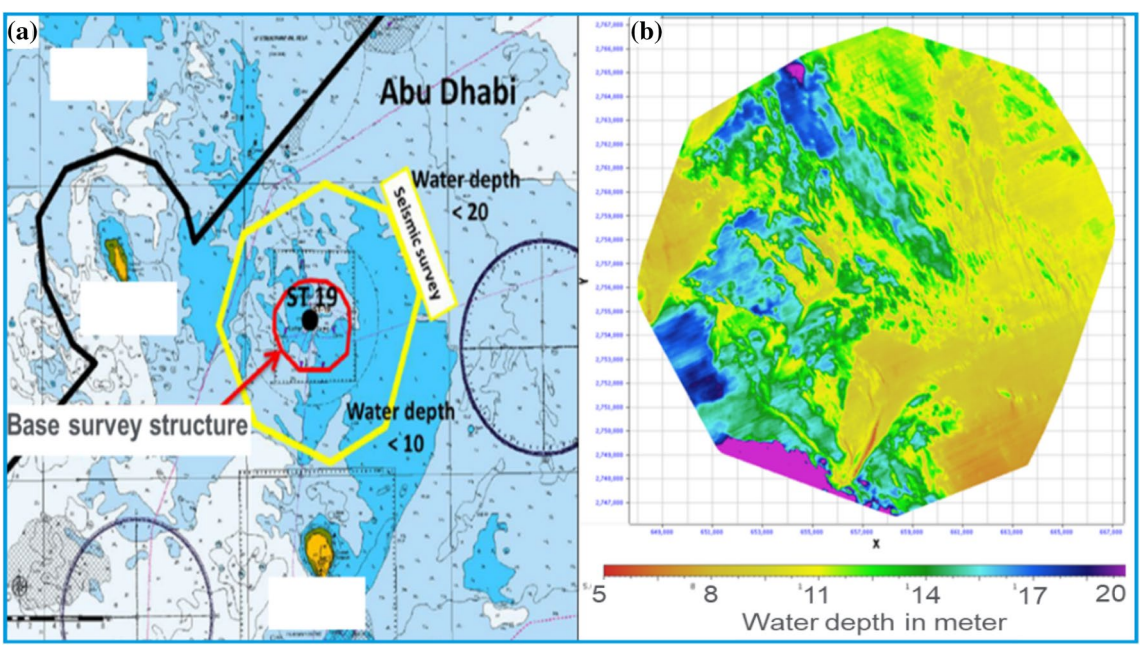

Fig. 1 **a** 4D seismic survey location map in the yellow polygon, and **b** 3D seismic survey bathymetry map

Table 1 Acquisition parameters of base and monitor survey

Acquisition parameters	Case I OBC 2010 (Base Survey)	Case I OBN 2020 (Monitor Survey)	Case II OBC 1994 (Base Survey)	Case II OBC 2014 (Monitor Survey)
Geometry	Orthogonal	Parallel	Parallel	Orthogonal
Source line interval (m)	250	50	50	100
Receiver line interval (m)	250	300	300	400
Source station interval (m)	25	25	25	25
Receiver station interval (m)	25	50	50	25
Bin size (m)	12.5 × 12.5	12.5 × 25	12.5 × 25	12.5 × 12.5
Maximum offsets (m)	3600	6000	3000	10,185 cut to 3000
Bin fold	192	2400	60	1200
Record length/sample rate (ms)	7000/2	7000/2	5000/2	6000/2

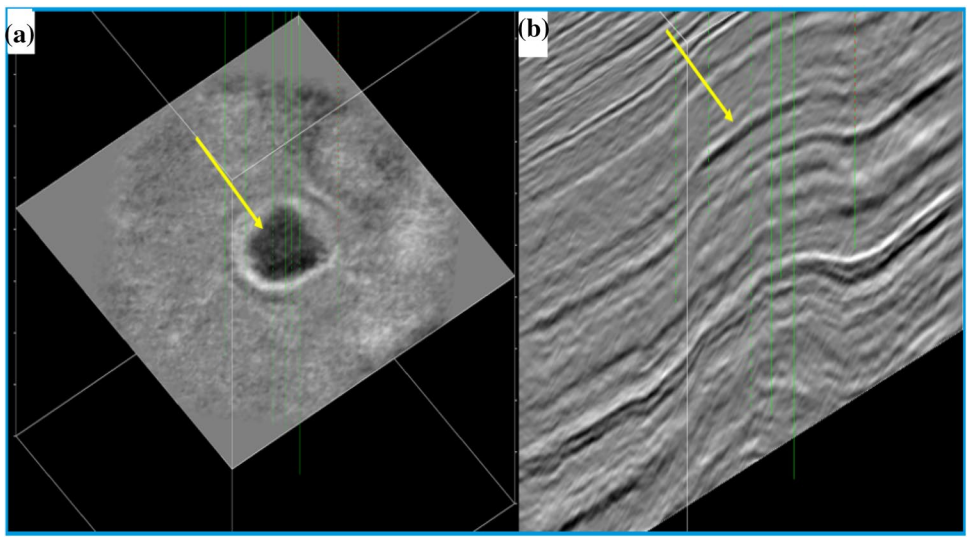

Fig. 2 Pre-stack depth migration seismic images with wells (vertical orange lines) from the baseline 3D survey **a** depth section at 2850 m and **b** vertical seismic section with the reservoir level highlighted by the yellow arrow at 2.85 km depth

Methodology

Theoretical Foundation

The least-squares Kirchhoff migration process, visco-acoustic modeling, which includes seismic absorption as described by the quality factor (conventionally denoted as Q) of the medium could be cascaded on the top of the LSM (Perrone et al. 2018).

In the Kirchhoff's demigration of the original imaging Kirchhoff can be transcribed as a linear operator:

$$d = Lr \tag{1}$$

In which d is the acquired seismic data, L is the acoustic operator of Kirchhoff modeling, while r is the reflectivity of the subsurface.

Resolving the inverse problem, $r = L^{-1} d$, provides the wanted subsurface reflectivity; nevertheless, the computation of this straight inverse is not feasible with the true seismic acquisition. The common alternative is to apply the adjoint, L^H of the forward operator, L to the seismic acquired data (Claerbout 1992):

$$m = L^H d \tag{2}$$

wherever m is the Kirchhoff migrated image.

This image will certainly suffer from migration artifacts and illumination issues since the inverse operator is not used. To overcome these shortfalls, the minimization of a least-squares cost function, $f(r) = \|d - Lr\|$, has been used and Nemeth et al. (1999) have developed a formulation that matches de-migrated modeled data with observed data to update the migrated image. Moreover, solution of the least-squares normal equations gives the least-squares approximation of the subsurface reflectivity r_{LS}:

$$r_{LS} = \left(L^H L\right)^{-1} L^H d \tag{3}$$

where is $L^H L$ referred as Hessian operator and Eq. (3) can be iteratively solved, via using the conjugate gradient

approaches. Earth variable elastic properties could lead to the absorption of seismic waves, which entitle amplitude attenuation and phase distortion. The conventional acoustic migration that undertakes these (Q) effects could be handled in either pre- or post-migration processing. However, the standard migration can, in fact, be altered to directly compensate for these effects (Xie et al. 2009), through applying amplitude boost and fixing phase distortion issues. Incorporating Q in least-squares migration takes a different route to resolve the previously mentioned data quality concerns issue for amplitude by altering the modeling in Eq. (1) to be:

$$d = L_Q r \tag{4}$$

where L_Q does represent the visco-acoustic Kirchhoff modeling operator (Wu et al. 2017). The least-squares cost function could be formulated,$f(r) = d - L_Q r^2$, and this could solve the normal equations to give a new style of Eq. (3) that encompasses the Q-compensation:

$$r_{LS} = \left(L_Q^H L_Q\right)^{-1} L_Q^H d \tag{5}$$

Migration and de-migration of multiple passes tangled in the iterative solution of Eqs. (3) or (5) are expensive from computation perspectives; however, a cost-effective method could be done by exchanging Eq. (2) into Eq. (3) to offer:

$$r_{LS} = \left(L^H L\right)^{-1} m \tag{6}$$

From this equation, it was found that the least-squares approximation of the reflectivity is an inverse Hessian,$(L^H L)^{-1}$ operator which is the filtered version of the migrated image. Subsequently, the application of the inverse Hessian matrix operator to the migration shall reduce the imaging artifact. Guitton (2004) proposed that this could be done with non-stationary matching filters following a de-migration/re-migration process.

The 4D metric seismic attributes are the most important tools for evaluating seismic repeatability when it is possible to perform a meaningful seismic 4D analysis. Inferior repeatability could doom the 4D analysis to failure. The 4D signal can be measured using the normalized root mean square (NRMS) attribute, which is defined as the difference between two normalized datasets RMS. NRMS is routinely used as a quality control measure for time-lapse data (Lecerf et al. 2015). The sensitivity of the NRMS value to the repeatability of the acquisition geometry has been described in several publications, e.g., Landrø (2006), Kragh and Christie (2002), and Eiken et al. 2003, who concluded that the final NRMS value is regularly used to quantify 4D signal quality. Typically, NRMS values are used without concern for the seismic data's seismic signal bandwidth. However, publications indicate a dependence of the NRMS value on the dominant seismic frequency of the data (Calvert 2005). NRMS values have been cited in many time-lapse case studies; an NRMS value of about 35% was reported in the Draugen field where water was successfully observed instead of oil (Koster et al. 2000). Two densely sampled surveys taken a few days apart improved the NRMS value from 15 to 6% with careful adjustment (Eiken et al. 1999).

(NRMS) classically deliberate the RMS difference of the two traces a_i and b_i within a given time window $t1 - t2$ given window, divided by their average RMS, expressed as a percentage (Kragh and Christie 2002):

$$NRMS = \frac{200\ x\ RMS\left(a_i - b_i\right)}{RMS(a_i) + RMS(b_i)}$$

Predictability is the cross-correlations within a time window divided by their autocorrelations summed product, expressed as a percentage. Predictability values lie in the range 0–100% (Detomo 2013),

$$\text{Predictability} = \frac{\left(\sum C_{bm}\right)(\tau)\ x\ \left(\sum C_{bm}\right)(\tau)}{\left(\sum C_{bb}\right)(\tau)\ x\ \left(\sum C_{mm}\right)(\tau)}$$

where C_{bm} denotes the cross-correlation between base and monitor traces b_t and m_t, respectively, and computed within time window $t1 - t2$ and τ (Tau) is a constant value.

For seismic acquisition with poor repeatability, predictability ranges from 0 to 65%, while perfect predictability should be above 85%. Predictability is sensitive to noise and Earth reflectivity, while NRMS is sensitive to general static, phase, or amplitude differences. (Detomo 2013).

4D Seismic Co-processing Workflow

The 4D processing workflow was designed to optimally handle different types of acquisition data and reveal the 4D signal with good confidence between the baseline and monitor survey. The 3D baseline survey was acquired as 3D OBC seismic in 2010 and the acquired data was processed in the same year. In 2018, the seismic data were fully reprocessed pre-stack time migration (PreSTM) and pre-stack depth migration (PreSDM), while the monitor survey was conducted as a 3D OBN seismic survey in 2020. The baseline survey pre-stack data were selected from the latest 2018 processing vintage, while the monitor survey pre-stack data used the 3D upgoing/downgoing deconvolution results prior to 5D regularization.

The two surveys were subjected to different 3D processing sequences, especially in the pre-processing phases before 5D regularization. In the baseline survey, noise from both the geophone and hydrophone was reduced separately, followed by conventional pre-processing, PZ summation of the collocated geophone and hydrophone, removal of the source signature/receiver-side ghost, and removal of

residual bubbles, cascaded by 3D predictive deconvolution. At the monitor, pre-processing includes global and local PZ calibration of the geophone and hydrophone, followed by upgoing and downgoing wave field separation as input to 3D up/down deconvolution, which resulted in a significant reduction in shallow water multiples. Source and receiver de-ghosting, guided waves, dipping wave noise attenuation, and deconvolution were applied in the up/down deconvolution. The 4D seismic co-processing started with the data before the 5D regularization. The above showed that the pre-processing was different for the baseline and monitor surveys, so the monitor survey had less multiple contaminations compared to the baseline seismic data. Regridding was the most essential step to obtain an updated similar geometry and a bin size of 12.5 × 25 m for the monitor survey, while the bin size of the baseline survey was 12.5 × 12.5 m to obtain a common grid with a bin size of 25 × 25 m.

Both datasets are then sorted into common offset vector (COV) tiles. The monitor study was prepared before 4D binning co-processing of the base and monitor by applying deabsorption phase Q and random noise reduction to the node-receiver domain. Seismic 4D data processing is a consecutive process that begins with 4D binning and synchronized 4D pre-stack processing; 4D binning increases spatial repeatability. Meanwhile, "simultaneous 4D pre-stack processing" develops common processing operators using cross-equalization as the fundamental method. After 4D binning, an additional step of noise reduction per COV was performed for monitor survey. For the two main seismic migration steps, 3D regularization was applied before conventional Kirchhoff pre-stack depth migration (KPSDM), while it was proved that least-square migration (LSM) works better than Kirchhoff migration without 3D seismic regularization.

In Case I, 4D seismic co-processing began in the middle of the processing sequence for the baseline and monitor surveys, whereas in Case II, 4D seismic co-processing began with the field data of baseline and monitor survey (Fig. 3).

Results and Discussion

In Case I, 4D seismic co-processing of baseline and monitor surveys was initiated with the input of 5D trace interpolation and regularization, and an offset limited to 3.2 km was used. The DSDR (Distance Source, Distance Receiver), which is the sum of the mispositioning of the sources and receivers from the baseline to the monitor survey, is commonly applied in the processing sequence to increase repeatability

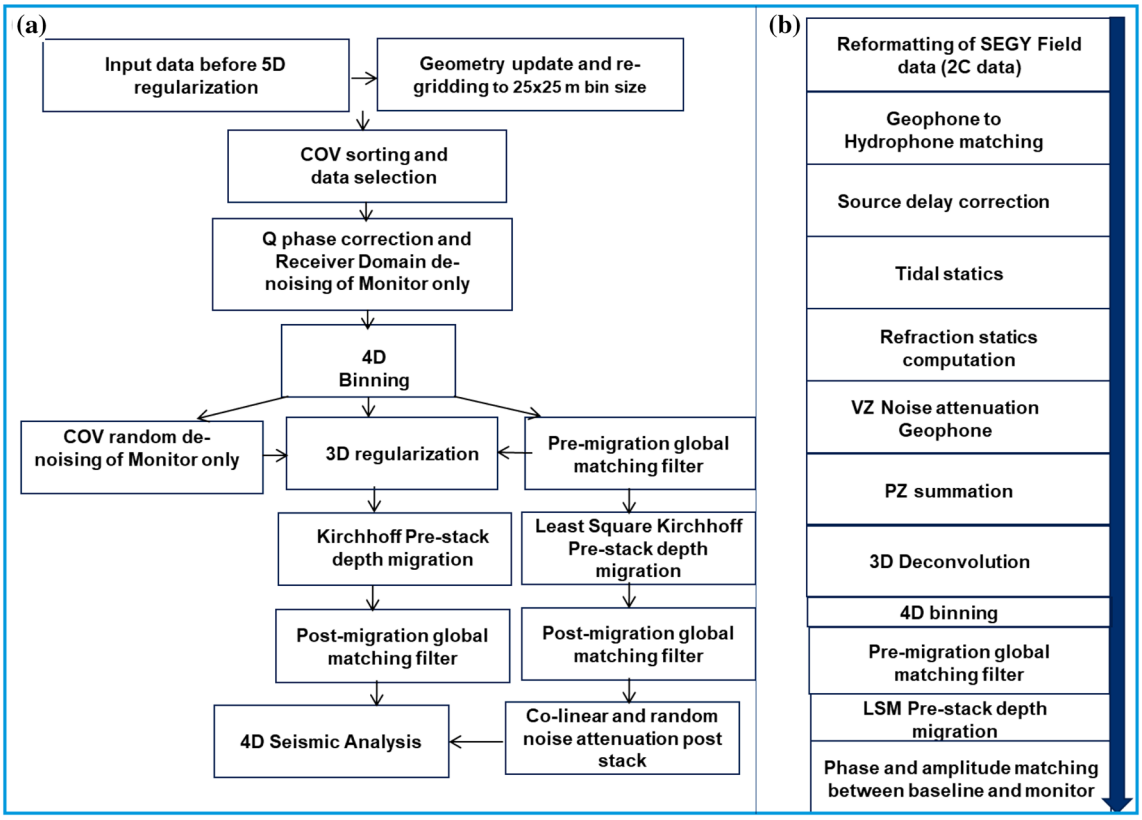

Fig. 3 The 4D Seismic co-processing workflow **a** Case I sequence and **b** Case II sequence

between the baseline and monitor surveys (Skinner et al., 2015).

The classical 4D binning approach, which compares traces with common midpoints, was tested against flexible 4D binning, allowing traces to be compared across offsets and midpoints to pair the best traces between base and monitor. Several 4D binning tests were performed using the DSDR criterion and 4 traces in each bin from each vintage were selected, but one difficulty was the choice of grid for binning. After several tests, the 25mx25m grid was finally chosen because it helped select pairs of traces that were more repeatable. Flexible binning parameters used were 50 m bin search range, an offset search range of 1000 m, and a maximum DSDR value of 350 m, resulting in a significant reduction in DSDR value with a mean value of less than 200 m. In the other Case II, macrobinning was performed using the adjacent offset classes of the 1994 baseline survey to select the retained traces with a DSDR value of less than 200 m for offset classes 1 to 16 and of less than 300 m for offset classes 17 to 62, followed by 5D Fourier bin regularization including noise attenuation. Because the geometry of the base and monitor surveys is not repeatable, 4D seismic co-processing was the way to approximate the base and monitor data in phase and amplitude to minimize the cross-equalization filter iterations and keep the 4D seismic signals intact. To close the repeatability gap, it was decided to test the pre-stack least-squares (LSM) depth migration algorithm against the Kirchhoff pre-stack depth migration algorithm (KPSDM).

The pre-stack seismic depth imaging workflow started with Kirchhoff KPSDM for the baseline and monitor survey, proceeded to dimigration of the original Kirchhoff depth imaging OVTs, and then applied least-square migration (LSM) to the baseline and monitor surveys. To compensate for the poor repeatability of the acquisition design between the base and the monitor with different source/receive coordinates, different azimuths, and a variety of obstacles, a least-square migration test was performed to de-migrate the monitor to the base coordinates.

To this end, both datasets were migrated recursively after pre-processing and de-migrated at each iteration with the calculation of the Hessian filter in the Curvelet domain to create a reflectivity model for each vintage. The base and monitor were then finally de-migrated to the baseline survey coordinates, with three iterations before the final reflectivity models were created.

The least-square migration result for the base and monitor without prior 3D regularization was quite clean compared to the KPSDM after 3D regularization. The difference of LSM between the base and monitor was much smaller than the difference of the KPSDM, proving that the seismic results of LSM are more repeatable. The depth slices of the reservoir at 2855 m show the same observation as mentioned above: the base and monitor LSMs are much cleaner than the KPSDM and show the crest of the reservoir structure with a very clear image (Fig. 4).

The diagnostic type of data quality in seismic processing is to look at the octave panels of seismic data before and after noise and multiple reductions to ensure that data quality is improved without signal/primary leakage in the seismic difference. The band pass filter was applied to the final migrated seismic volumes of both KPSDM and LSM and produced seismic frequency panels with six octaves, namely 2–4, 4–8, 8–16, 16–32, 32–64, and 64–128 Hz. The frequency panels of the KPSDM were all noisier than those of the LSM; also, 16–32 Hz range is the better octave with less noise than the high-frequency end and fewer multiples than the low-frequency end of the seismic bandwidth (Fig. 5).

After LSM proved to be the best migration algorithm for 4D seismic co-processing imaging, we next extracted

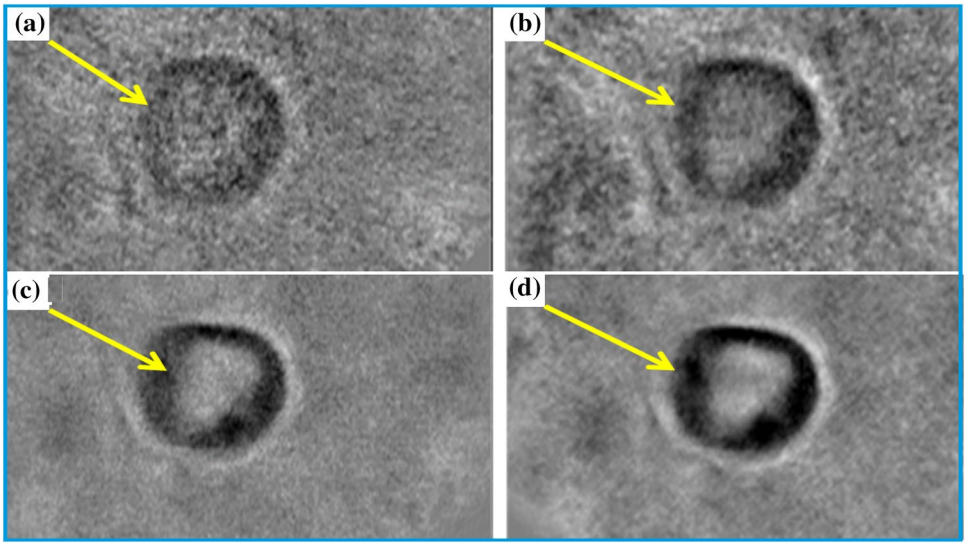

Fig. 4 Depth slices of the reservoir level at 2850 m: **a** base KPSDM, **b** base LSM, **c** monitor KPSDM, and **d** monitor LSM. The crest of the structure is indicated by a yellow arrow

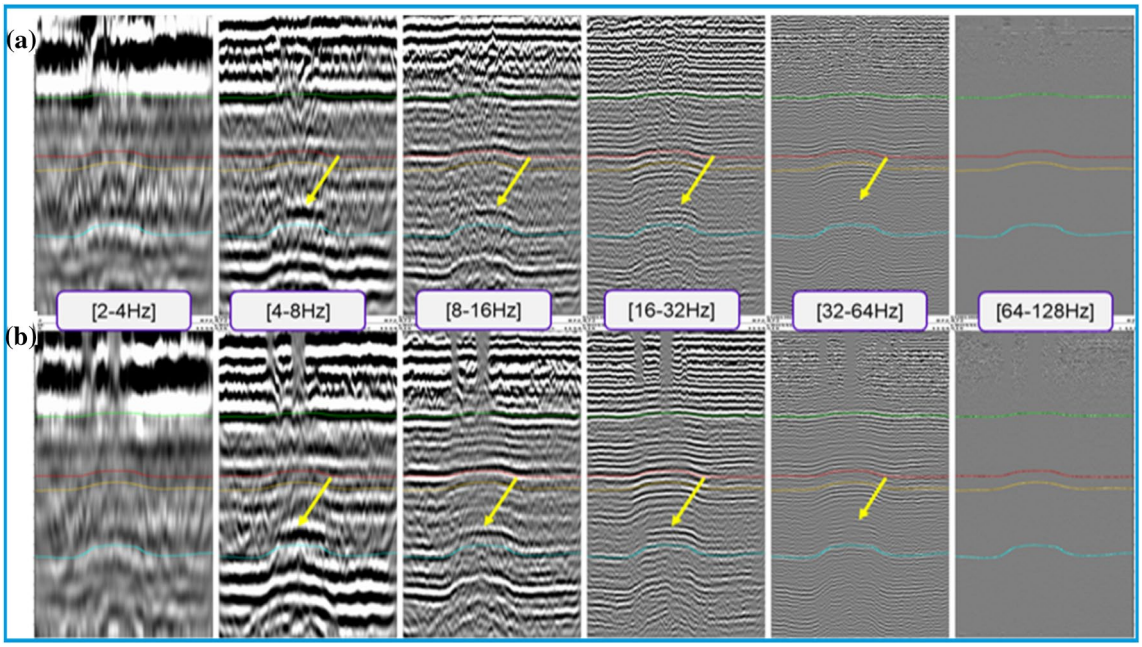

Fig. 5 Comparison of seismic frequency octaves of the monitor survey: **a** KPSDM and **b** LSM. The yellow arrow points to the peak of the reservoir level

seismic amplitude and phase attributes, which are extremely important for identifying the 4D signal. Amplitude and phase attributes are physical attributes directly related to seismic wave propagation and lithologic changes. These attributes mainly represent the contrast of acoustic impedance and thus reflectivity. They are also useful in identifying bright spots, direct hydrocarbon indicators, and gas accumulations (Subrahmanyam and Rao 2008). The instantaneous phase is measured in degrees (-π,π), is independent of amplitude, and indicates continuity and discontinuity of events. In contrast, the cosine of the instantaneous phase indicates embedding and discontinuity very well (Subrahmanyam and Rao 2008). The extracted cosine attribute of the instantaneous phase over the LSM seismic volumes in the 1500 ms time slice of the monitor shows visible discontinuities at the structure's apex compared to the smoothed outlines of the structure crest of the baseline survey (Fig. 6).

Upon further investigation of the aforementioned discontinuities in the time slice of the cosine of the instantaneous phase, the corresponding geometric boundary attribute (seismic coherence) was extracted to determine if the structure of the domain indicated a possible influence on the mechanism of 4D signal generation. It is clearly seen that the time slice of the seismic coherence attribute at 1500 ms of the reservoir

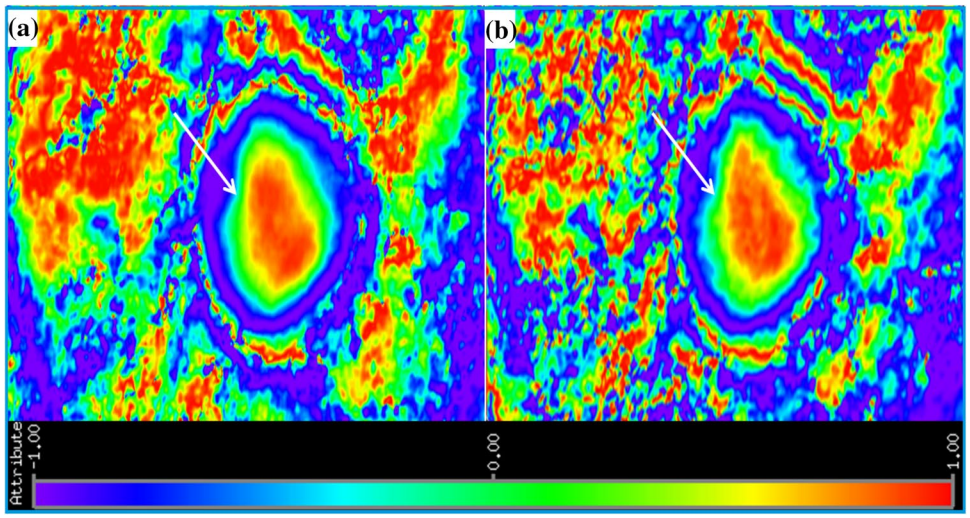

Fig. 6 3D seismic attribute of the final migrated LSM stack; cosine of instantaneous phase at a time slice of 1500 ms **a** baseline image **b** monitor image. The white arrow points to the crest of the structure's reservoir

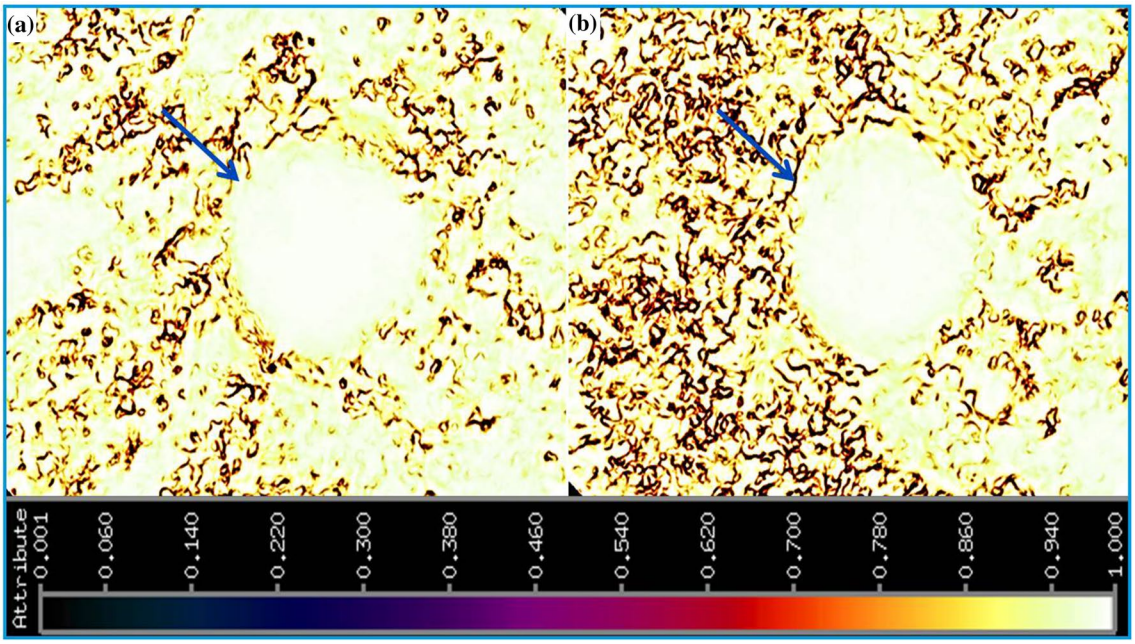

Fig. 7 3D seismic coherency attribute of the cosine of the instantaneous phase volume at 1500 ms **a** baseline image and **b** monitor image. The blue arrow points to the crest of the structure

level of the monitor survey shows strong faulting and fault lineaments around the periphery of the crest of the structure (Fig. 7). This matter could be evidence that the 4D signal in the reservoir is more or less coherent with the structural scheme.

To cope with the booming 4D broadband seismic technology, it is important to understand the performance of the repeatability 4D metric attributes. LSM data have been shown to have significantly lower NRMS than KPSDM data, although the main differences between base and monitor are indistinguishable in both models. The 4D metric attributes were extracted from the final migrated LSM stack volumes and compared to the KPSDM seismic datasets. The NRMS attribute of the migrated LSM stack volume showed less than 50% NRMS at the crest of the structure in the 1500 ms time slice with a wider structure closure than the seismic KPSDM dataset, which showed higher NRMS at both the crest and flanks of the structure (Fig. 8).

The predictability attribute of the 4D metric showed that the predictability of the LSM seismic volume reached almost 100%, especially at the apex of the reservoir structure with wider closure, better than the KPSDM seismic volume (Fig. 9).

We extracted frequency panels of different seismic frequency octaves and found that the baseline and monitor surveys' usable dominant frequency range is about 30 Hz. With this dominant frequency range, the noise component was significantly reduced and the matching between the baseline and monitor surveys was improved. The final migrated LSM stack depth was converted to time using the appropriate interval velocity model and filtered out by a high-cut filter at 30 Hz of the seismic bandwidth. The filtered stack of the monitor looks much closer in amplitude to the baseline dataset than the stacks of the full seismic bandwidth. In addition, the difference between the base and monitor surveys of the band-limited frequency range exhibits a strong amplitude contrast at the peak of the structure compared to the difference in the volume of the full seismic bandwidth (Fig. 10).

The Case study I, with its incomplete 4D seismic co-processing workflow, showed that the data between the baseline and monitor studies vary in signal from 30 Hz. In contrast, the noise spectrum of the monitor survey is much higher than that of the baseline survey (Fig. 11 a&b). In contrast, in the II case, the signal spectrum of the baseline and monitor surveys are quite identical, as is the noise level (Fig. 11 c&d).

In addition, the content of the multiples may differ significantly between the baseline and monitor surveys if the preprocessing phase in the 4D seismic co-processing workflow is not performed uniformly. In Case I, the baseline survey autocorrelation window is heavily contaminated with shallow water multiples, while the monitor survey autocorrelation window contains significantly fewer multiples after applying up/down deconvolution (Fig. 12 a&b). In contrast, 4D seismic co-processing of the baseline and monitor survey began with the field raw seismic data in the second case. The full seismic 4D co-processing paved the way to clean the

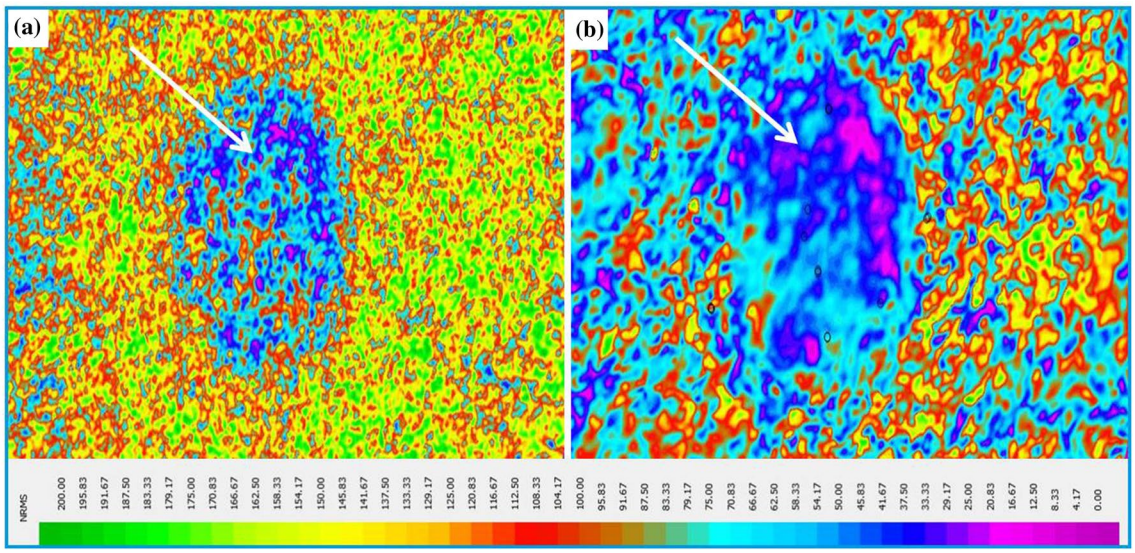

Fig. 8 Comparison of 4D metric NRMS attribute maps extracted at the 1500 ms reservoir level **a** KPSDM, **b** LSM. The ridge of the structure is indicated by a white arrow

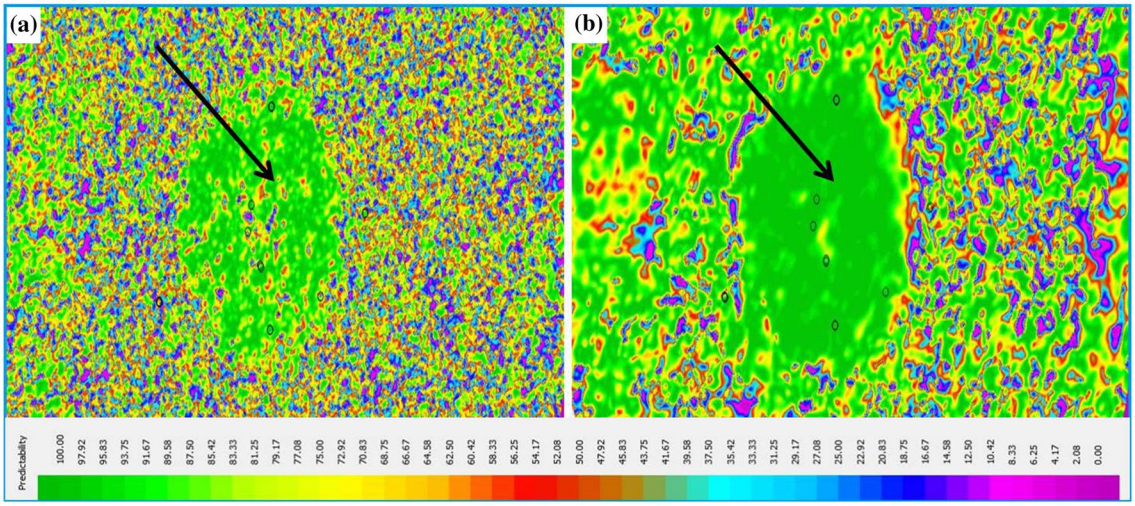

Fig. 9 Comparison of attribute maps of 4D metric predictability extracted at the 1500 ms reservoir level **a** KPSDM, **b** LSM. The black arrow points to the crest of the structure

data from noise and multiples and to align the seismic data quality of the baseline and the monitor survey. (Fig. 12 c&d).

Quantification of the difference between the baseline survey and the monitor survey for KPSDM and LSM is done by plotting NRMS against predictability. NRMS is a standard measure of 4D seismic repeatability (noise), while predictability measures repeatability between the baseline and monitor seismic datasets. Cross-plotting compared the NRMS with the predictability of KPSDM and the final migrated seismic volumes of the LSM, limiting the frequency range to 30 HZ. The cross-plot was extracted for both datasets on the time window with 40 ms above and below the reservoir seismic horizon. It is found that the NRMS values of the KPSDM are in the range of 60–85% NRMS, which is a significantly high 4D, noise level. It also shows moderate predictability with a mean value of more than 80% (Fig. 13).

The LSM shows less NRMS % 4D noise with a value of about 45%, while the predictability reaches almost 100%, which is much higher than the KPSDM (Fig. 14). Therefore, the LSM does look more repeatable than the KPSDM seismic migration results.

Comparing the cross-plotting of the partial 4D seismic co-processing of Case I with the full 4D seismic

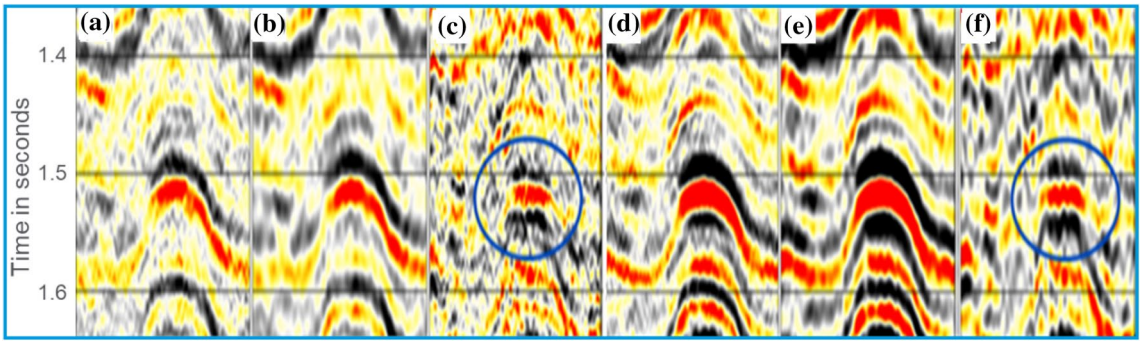

Fig. 10 Final LSM migrated stack 3D seismic volumes, vertical seismic section of LSM **a** monitor with full seismic bandwidth, **b** base with full seismic bandwidth, **c** difference with full seismic bandwidth, **d** base 30 Hz **e** monitor 30 Hz volumes, and **f** the 30 Hz difference. The blue circle indicates the level of the reservoir

co-processing of Case II, we found that in Case II 4D seismic co-processing, both KPSDM and LSM have the same 100% predictability, while the NRMS mean of KPSDM is almost 15% (Fig. 15a). However, the NRMS mean for the final migrated stack volume of LSM reaches nearly 12% (Fig. 15b).

The LSM does not require 3D/5D regularization and trace interpolation as input, as this would compromise the effectiveness of the LSM. A band-limited seismic frequency bandwidth clearly shows the improvement of 4D seismic repeatability since the higher frequencies are mostly overwhelmed by random noise. Moreover, the low frequencies have mudroll seismic waves (coherent noise) and multiple reverberations in shallow water. In Case I, the non-repeatable acquisition parameters as well as the blended sources seismic acquisition mode of the 3D OBN monitor survey in 2020, compared to the flip-flop acquisition of the baseline 3D OBC survey, pose a major challenge to 4D seismic co-processing. The start of seismic co-processing in the intermediate processing phase reduced the optimization of the processing sequence to bring the seismic datasets of the monitor survey close to the baseline survey in terms of seismic data quality.

Since the start of 4D co-processing of up/down Decon, it was not possible to calculate the variation in water column velocity because the acquisition time of the baseline and monitor measurements was different, and tidal statics could not be calculated either. In addition, after the up/down Decon, direct arrivals were removed because they parallel the seismic noise of the guided waves. This made it impossible to calculate the residual statics of the common surface consistency, which is an advantage for

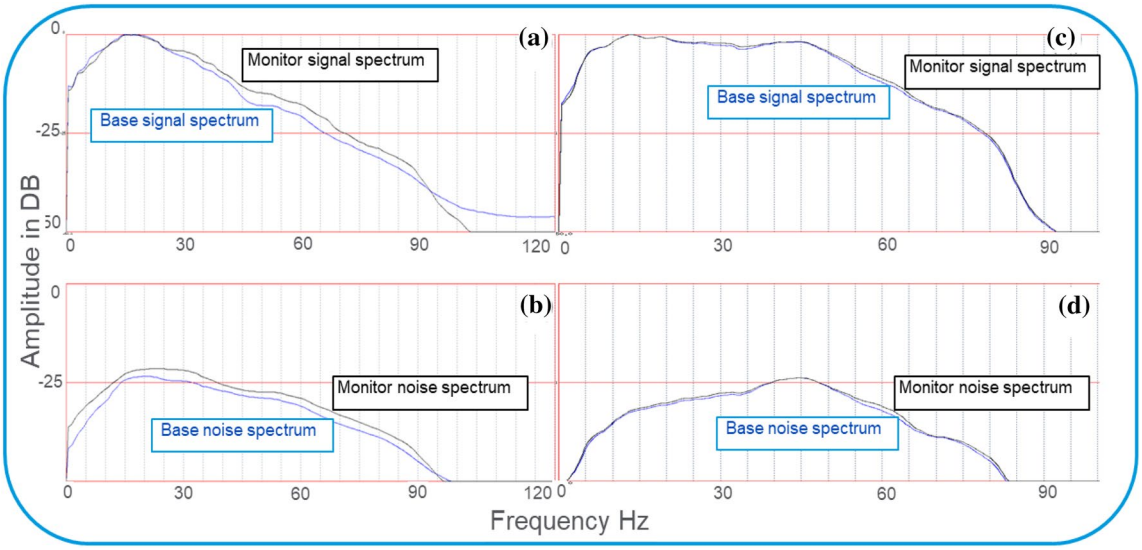

Fig. 11 Spectral analysis of the signal-to-noise ratio on a subline of the 3D seismic volume **a** Case I signal spectrum, **b** Case I noise spectrum, **c** Case II signal spectrum, and **d** Case II noise spectrum

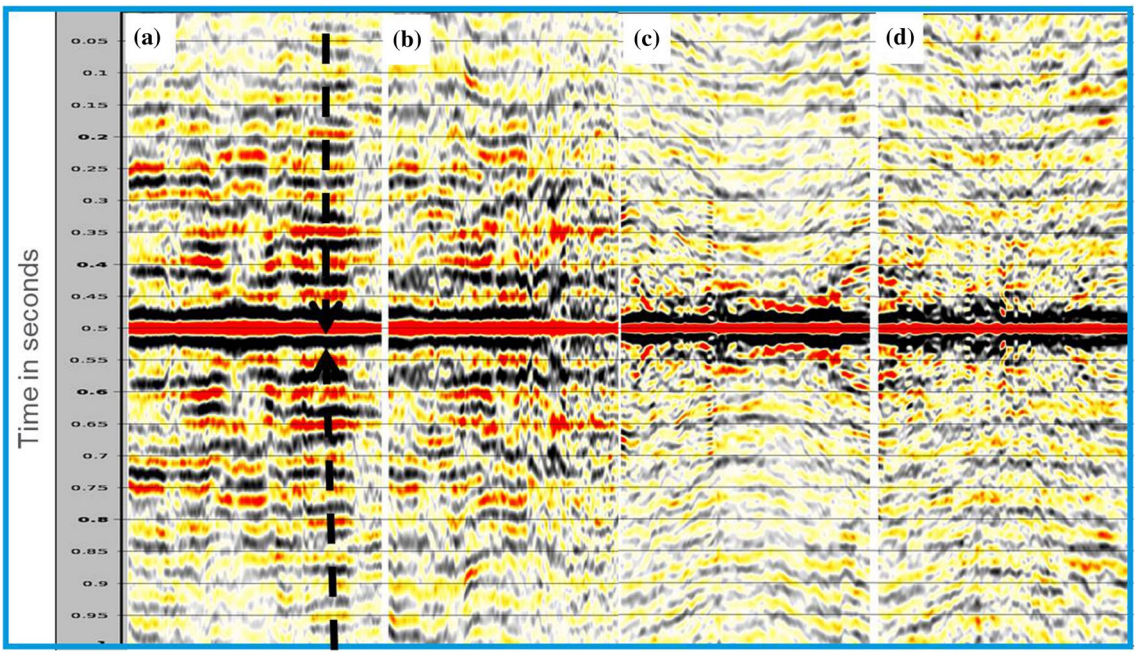

Fig. 12 4D autocorrelation window of an inline extracted over the 3D seismic volumes **a** Case I Baseline Survey and the black dashed line points to terrain with periodic multiples, **b** Case I Monitor Survey, **c** Case II Baseline Survey, and (d) Case II Monitor Survey

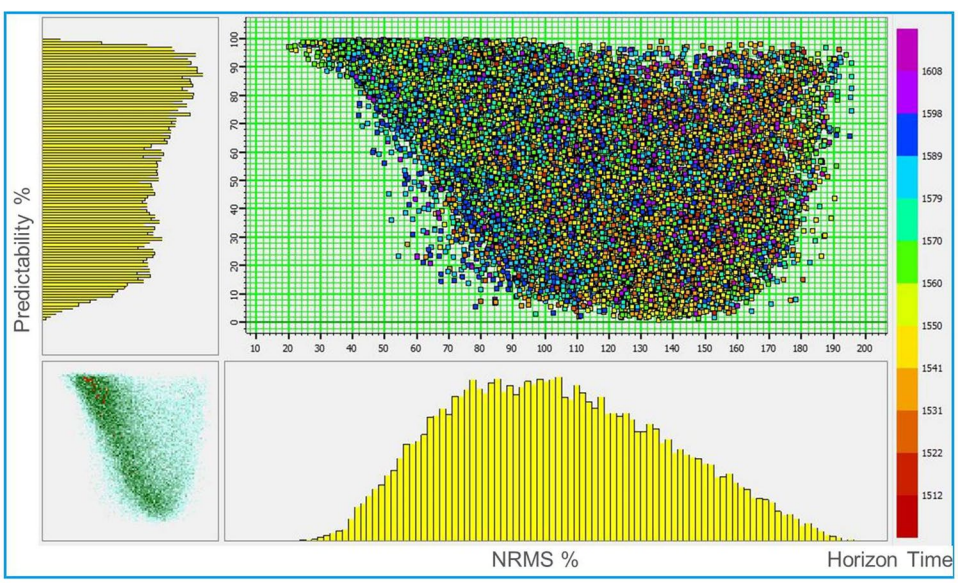

Fig. 13 4D cross-plot between NRMS% and predictability % with histograms of NRMS and predictability in the upper and lower reservoir horizon window of the final migrated seismic volume of the KPSDM

matching baseline and monitoring measurements in the overburden level. In contrast, at the reservoir level, the time differences between the baseline and the monitor and the amplitude differences are the diagnostic 4D attributes.

In the Case II, 4D seismic co-processing was started from the field records of baseline and monitor survey. Pre-processing, including noise reduction and static computation with predictive 3D deconvolution, enabled successful overburden phase and amplitude matching, and reservoir level is retained intact. The NRMS histograms are indicative of the 4D noise level, in Case I, the KPSDM seismic volume, the NRMS mean is close to 80%, while in the LSM seismic volume, it dropped to less than 50%.

On the other hand, in the Case II, where the full 4D co-processing was used, the NRMS mean of the 4D noise level was significantly reduced to almost 10%. The reduction of 4D noise by more than 35% in the Case II study confirms the assumption that the good survey repeatability achieved through the 4D seismic co-processing is not due to LSM alone, but that full seismic 4D co-processing using the LSM

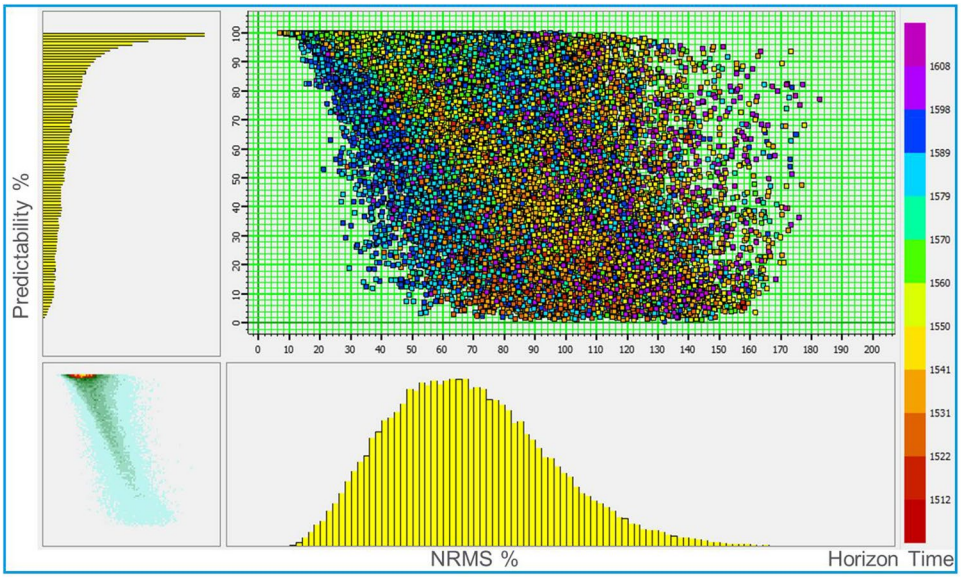

Fig. 14 4D cross-plot between NRMS% and predictability % with histograms of NRMS and predictability in the upper and lower reservoir horizon window of the final migrated seismic volume of the LSM

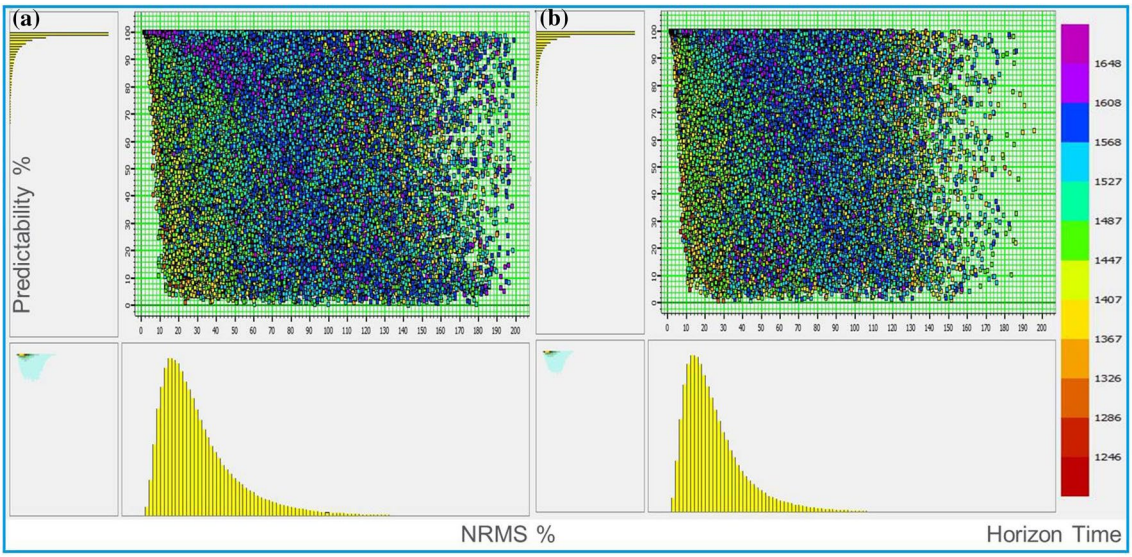

Fig. 15 Case II; 4D cross-plot between NRMS% and predictability % with histograms of NRMS and predictability in the upper and lower reservoir horizon windows **a** KPSDM final migrated seismic volume and **b** LSM final migrated seismic volume

algorithm for pre-stack depth migration is recommended to be followed, regardless of acquisition repeatability.

Conclusion

We infer that with large differences in the noise and multiples content of the baseline and monitor surveys, the results of the global and local matching filters in the overburden are extremely poor, which in turn will not improve the scarce seismic acquisition repeatability we have for Case study I in particular. This suggests that the same preprocessing and deconvolution should be applied to the baseline and monitor surveys.

4D seismic metric attributes and quantification of changes in NRMS and predictability are important to measure how 4D seismic co-processing could enhance seismic acquisition repeatability. LSM's depth migration algorithm is better suited for 4D seismic co-processing than KPSDM. The deliberate full seismic 4D co-processing starting from the seismic field records is more accurate and robust, and thus far more repeatable than partial 4D seismic co-processing using KPSDM or LSM.

This study shows that in 4D seismic, working with seismic wiggle traces by analyzing vertical and horizontal time sections is no longer used merely to indicate that the base and monitor differences are pure 4D signals. As this research progresses, the mechanism of 4D signal generation will be investigated through integrating seismic co-processing results, data validation, reservoir simulation models, and reconciliation with the oil and gas production history matching of the field.

Acknowledgements The authors thank the management of ADNOC (Abu Dhabi National Oil Company) and USM (Universiti Sains Malaysia) for permission to publish this work. We also thank the CGG processing team in CGG HQ in Paris and in Abu Dhabi for carrying out the processing with the help of CGG Processing Geovation II. I would also like to thank Karim El Saadni, Project Manager at WesternGeco, for his help.

Funding This project was funded by Short-Term Research Grant titled "Seismic Imaging for High-resolution Subsurface. Structure Interpretation using Reflection and Diffraction Data," Grant No (304/PFIZIK/6315489).

Declarations

Conflict of interest: The authors declare that they have no conflict of interest.

References

Ayeni G, Biondi B (2010) Target-oriented joint least-squares migration/inversion of time-lapse seismic data sets, Geophysics, May 2010. Soc Explor Geophysicists. https://doi.org/10.1190/1.3427635

Calvert R (2005) 4D Technology: Where are we, and where are we going? Geophys Prospect 53:161–171

Claerbout J (1992) Earth sounding analysis: processing versus inversion: Blackwell Scientific Publications

Detomo R (2013) 4D time lapse seismic reservoir monitoring of African reservoirs, SEG Regional Honorary Lecturer

Eiken O, Waledmar P, Schonewille M, Haugin G, Duijndam A (2003) A proven method for acquiring highly repeatable towed Streamer seismic data. Geophysics 68:1303–1309. https://doi.org/10.1190/1.1598123

Eiken O, Waledmar P, Schonewille M, Haugin G, and Duijndam A (1999) A proven concept for acquiring highly repeatable towed Streamer seismic data: 61th Conf. &Tech. Exhibit. EAGE, Exp. Abs. 1–40.

Fischer D, Teichmann E, Blekastad H, Moen SA, Sollie I, and H, Smith P (2013), Value creation by a long-term time-lapse Seismic processing approach, FB, volume 31, Oct. 2013.

Gray SH (1997) True-amplitude seismic migration: A comparison of three approaches. Geophysics 62(3):929–936

Guitton A (2004) Amplitude and kinematic corrections of migrated images for non-unitary imaging operators: Geophysics, v. 69, p. 1017– 1024.

Huang S, Wang Z, Wang, M, and Khalil A (2017) Application of least-squares pre-stack depth migration in complex geology around the World, FB, 36: 43–48.

Kendall CG. and Alsharhan AS (2013) Reservoir Character of Carbonate/Evaporite Oil Fields of the Middle East, a Response to Depositional Setting, and Accommodation Space *Adapted from poster presentation given at AAPG 2013 Annual Convention and Exhibition, Pittsburgh, Pennsylvania, May 19–22, 2013.

Koster K, Gabriles P, Hartung M, Verbeek J, Deinum G, Staples R (2000) Time-lapse seismic surveys in the North Sea and their business impact. Lead Edge 19(19):286–293

Kragh E, Christie P (2002) Seismic repeatability, normalised RMS and predictability. Lead Edge 21:640–647. https://doi.org/10.1190/1.1497316

Landrø, M (2006), Future challenges and unexplored methods for 4D seismic analysis: RECORDER, Mar 2006, VOL. 31 NO. SPECIAL.

Lecerf D, Burren J, Hodges Ed, and Barros C, (2015) Repeatability measure for broadband 4D seismic, SEG New Orleans Annual Meeting. https://doi.org/10.1190/segam2015-5927745.1.

Liu, S., Liu, F., Chemingui, N., Valenciano, A., and Long, A., (2018), Least-squares full-wavefield migration. The Leading Edge Special Section: Advancements in 3D seismic processing, 46–51, https://doi.org/10.1190/tle37010046.1.

Lumley D, Adams, DC, Meadows M, Cole S, and Wright R (2015) 4D seismic data processing issues and examples: SEG Technical Program Expanded Abstracts, 22, 1394–1397.

Mitra PP, Murty JVSSN, Josyulu, BS Menon M. and Sen G (2007), Post Stack 4D Seismic Data Conditioning and Validation to Map the Changes in Fluid Phase, GEOHORIZONS December 2007/5.

Nemeth T, Wu C. and Schuster GT (1999), Least-squares migration of incomplete reflection data. Geophysics, 64 (1), 208–221. https://doi.org/10.1190/1.1444517.

Perrone F, Graham R, Lorenzo C, Andrew R, Arash J, and Karen P, (2018), Applications of Kirchhoff Least-Squares Migration: Towards Reservoir Imaging, adapted from extended abstract based on oral presentation given at AAPG International Conference and Exhibition, London, England, October 15–18.

Prucha M, Biondi B (2002) Subsalt event regularisation with steering filters: 72nd Annual International Meeting. SEG, Expanded Abstracts. https://doi.org/10.1190/1.1816859

Ross CP, Cunningha, GB. and Weber DP (1996) Inside the cross sequalisation black box: the leading edge, 15, NO. 11, 1233-1240.

Schuster GT (1993) Least-squares crosswell migration. SEG Tech Program Expand Abstr. https://doi.org/10.1190/segam2012-1425.1

Shao G, Dongping Z, Rongxin H, Ping W, Bertram N, Pedro P, Kareem V (2017) Least-squares Q migration: the path to improved seismic resolution and amplitude fidelity. SEG Tech Program Expand Abstr. https://doi.org/10.1190/segam2017-17742644.1

Subrahmanyam D, and Rao PH, (2008), Seismic Attributes- A Review, 7th International conference and Exposition on Petroleum Geophysics, Hyderabad, 2008.

Valenciano A, (2008) Imaging by Wave-Equation Inversion: PhD thesis, Stanford University.

Wang Z. Huang R., Xuan Y, Xu Q, Morton, S, and Kuntz B (2017) Improving OBS-streamer 4D imaging by least-squares migration, SEG International Exposition and 87th Annual Meeting.

Wu X, Wang Y, Xie Y, Zhou J, Lin D, Casasanta L (2017) Least square Q-Kirchhoff migration: implementation and application: 79th EAGE conference and exhibition, EAGE, Extended Abstracts Tu A1 08

Xiao-Dong S, Zhong-Hui G. and Zhen-Chun L (2017) Conjugate gradient and cross-correlation based least-square reverse time migration and its application, App geophys, Vol.14 No.3 (Sep. 2017) https://doi.org/10.1007/s11770-017-0626-9.

Xie Y, Xin SK, Sun J, Notfors C, Biswal AK and. Balasubramaniam MK (2009), 3D Prestack depth migration with compensation for frequency dependent absorption and dispersion: 79th Annual International Meeting, SEG, Expand Abstr, 2919–2923.

Zhang Y, Zhang H (2009) A stable TTI reverse time migration and its implementation. SEG Tech Progr Expand Abstr. https://doi.org/10.1190/1.3255429